Measurements of the Branching Ratio of the $K_L \to \pi^+\pi^-$ decay with the KLOE Detector

M. Antonelli [a], M. Testa [b]

[a] *Laboratori Nazionali di Frascati dell'INFN, Frascati, Italy.*

[b] *Dipartimento di Fisica dell'Università "La Sapienza" e Sezione INFN, Roma, Italy.*

Abstract

From a sample of about 10^9 ϕ mesons produced at DAΦNE, we have selected K_L mesons tagged by observing $K_S \to \pi^+\pi^-$ decays. We present results on the $K_L \to \pi^+\pi^-$ branching ratio. A determination of the η^{+-} is also given.

1 Analysis strategy

At a ϕ factory a clean sample of nearly monochromatic[1] K_L's can be selected by identification of K_S decays. This procedure is called K_L "tag". The absolute K_L branching ratios can be determined using this sample by counting the fraction of K_L decays in each channel and correcting for acceptances, reconstruction efficiencies and background. However, the tagging procedure is not perfect, because the tagging efficiency depends slightly on the decay channel of the K_L. The sources of these differences in the tagging efficiency are described in details in Sec. 2.
The dependence of the tagging efficiency on the K_L decay channel can be evaluated by defining the *tag bias* as the ratio of the tagging efficiency for $K_L \to k$ in the fiducial volume (FV) to the overall tagging efficiency, determined without regard to the final state of the K_L. The tag bias for channel k is thus $\varepsilon_{\mathrm{tag}_k} / \varepsilon_{\mathrm{tag}_{\mathrm{tot}}}$, and

$$\mathrm{BR}(K_L \to k) = \frac{N_k}{\varepsilon_{\mathrm{tag}_k}/\varepsilon_{\mathrm{tag}_{\mathrm{tot}}}\, N_{\mathrm{tag}}\, \varepsilon_{\mathrm{FV}}\, \varepsilon_{\mathrm{rec}k}}, \tag{1}$$

where N_k is the number of K_L decays to k, N_{tag} is the number of tagged K_L's, $\varepsilon_{\mathrm{FV}}$ is the geometrical efficiency of the fiducial volume, and $\varepsilon_{\mathrm{rec}k}$ is the reconstruction

[1] ϕ mesons at DAΦNE are infact produced nearly at rest with a small horizontal momentum of about 12 MeV.

efficiency.

The strategy of the measurement of the BR($K_L \rightarrow \pi^+\pi^-$) is driven by the requirement of reducing the systematic error due to the tag bias evaluation. For this purpose, the measurement of the BR($K_L \rightarrow \pi^+\pi^-$) is performed by measuring the ratio $BR(K_L \rightarrow \pi^+\pi^-)/BR(K_L \rightarrow \pi^\pm\mu^\mp\nu)$ given by

$$\frac{\mathrm{BR}(K_L \rightarrow \pi^+\pi^-)}{\mathrm{BR}(K_L \rightarrow \pi^\pm\mu^\mp\nu)} = \frac{N_{\pi^+\pi^-}}{\varepsilon_{\mathrm{tag}_{\pi^+\pi^-}}\,\varepsilon_{\mathrm{rec}\pi^+\pi^-}} \Big/ \frac{N_{\pi^\pm\mu^\mp\nu}}{\varepsilon_{\mathrm{tag}_{\pi^\pm\mu^\mp\nu}}\,\varepsilon_{\mathrm{rec}\pi^\pm\mu^\mp\nu}} \qquad (2)$$

where

- $\varepsilon_{\mathrm{tag},k} = \frac{N_{\mathrm{tag}\,k}}{N_{\mathrm{prod}\,k}}$, the tagging efficiency, is the ratio between the number of $K_L \rightarrow k$ decays tagged and the number of $K_L \rightarrow k$ decays generated. It includes the trigger efficiency $\varepsilon_{\mathrm{trig},k}$;
- $\varepsilon_{\mathrm{rec},k} = \frac{N_{\mathrm{rec}\,k}}{N_{\mathrm{tag}\,k}}$, the reconstruction efficiency, is the ratio between the number of reconstructed $K_L \rightarrow k$ decays and the number of tagged $K_L \rightarrow k$ decays.

The similar topology of the decays (both of them contain two charged particles) and the momenta overlap of the decay particles allow in fact a partial cancellation of the factor $\varepsilon_{\mathrm{tag}\pi^+\pi^-}/\varepsilon_{\mathrm{tag}\pi\mu\nu}$.
As the reconstruction efficiency depends on the particle momentum, also the ratio $\varepsilon_{\mathrm{rec}\pi^+\pi^-}/\varepsilon_{\mathrm{rec}\pi\mu\nu}$ partially cancels out.
The knowledge of the K_L's lifetime affects the geometrical efficiency $\varepsilon_{\mathrm{FV}}$: The 0.8% current accuracy on the K_L lifetime [3] [6] [7] leads to a 0.64% uncertainty on the absolute branching ratio measurement. Therefore, as the geometrical efficiency is identical for different channels, the measurement of the ratio BR($K_L \rightarrow \pi^+\pi^-$)/BR($K_L \rightarrow \pi^\pm\mu^\mp\nu$) is independent on the K_L's lifetime.

The fiducial volume used for the analysis is defined by:

$$30\,\mathrm{cm} < r_{xy} < 150\,\mathrm{cm}; \qquad |z| < 120\,\mathrm{cm},$$

where (x, y, z) are the coordinates of the K_L decay vertex position. Since the mean K_L decay length is in KLOE 340 cm, the FV contains $\sim 26\%$ of the K_L decays. The FV has been chosen *a posteriori* by requiring stability of the result, as it will be explained in Sec. 4. In fact the statistical error decreases with a larger FV, but the uncertainties related to the K_L nuclear interactions in the beam pipe wall ($r \simeq 10\,\mathrm{cm}$) and on drift chamber wall ($r_{xy} \simeq 25\,\mathrm{cm}$) as well as the data-MC discrepancies at low and high r_{xy} requires a FV which lies completely within the drift chamber (Sec. 4).

The value of $BR(K_L \to \pi^+\pi^-)$ is finally obtained using $BR(K_L \to \pi^\pm\mu^\mp\nu)$ from KLOE [6].

2 Tagging

The K_L tagging algorithm is fully described in Ref. 6, only the relevant aspects will be given in the following. Candidate events are identified by the presence of a $K_S \to \pi^+\pi^-$ decay. We require a vertex with two tracks of opposite curvature with origins within a cylindrical fiducial volume of radius $r_{xy} < 10$ cm and length $\Delta z < 20$ cm, centered on the collision region, as determined for each run using Bhabha events. The two-track invariant mass, in the pion mass hypothesis for both tracks, must be within 5 MeV of $\mathrm{m_K}$. The magnitude of the total momentum of the two tracks must be within 10 MeV of the value expected from two-body Φ decay kinematics and the value of $\mathbf{p}_\Phi$. If more than one vertex satisfies these criteria, that closest to the nominal Φ vertex position is identified as the $K_S \to \pi^+\pi^-$. The K_L momentum, p_{K_L}, is obtained from the kinematics of the $\Phi \to K_S K_L$ decay, using the K_S direction reconstructed from the measured momenta of the decay tracks and the known value of $\mathbf{p}_\Phi$. The resolution is dominated by the beam-energy spread, and amounts to about 0.8 MeV/c. The position of the Φ production point, $\mathbf{x}_\Phi$, is determined as the point of closest approach of the K_S momentum, propagated backwards from the K_S vertex, to the beam line. The K_L line of flight (*tagging line*) is then constructed from the K_L momentum, $\mathbf{p}_{K_L} = \mathbf{p}_\Phi - \mathbf{p}_{K_S}$, and the position of the production vertex, $\mathbf{x}_\Phi$.

The tagging procedure is not perfect, because the tagging efficiency depends slightly on the evolution of the K_L (see also Ref. 6). We include events in which the K_L interacts in the calorimeter, escapes the detector, or decays to any final state. The difference in tagging efficiency in each case depends on the tagging algorithm; the minimization of such differences is used to optimize the tagging criteria.

In order to understand the advantage of normalizing the BR$(K_L \to \pi^+\pi^-)$ to the BR$(K_L \to \pi\mu\nu)$, it is worthwhile to describe the main sources of the dependence of the tagging efficiency on the K_L decay channel.

The main source of tag bias is the dependence of the trigger efficiency on the K_L behavior. The hardware calorimeter trigger [10], which requires two local energy deposits above some threshold (50 MeV on the barrel and 150 MeV on the end caps), is used for the present analysis. The trigger efficiency is essentially 100% for events in which the K_L decays to $\pi^0\pi^0\pi^0$, between 85-95% for events in which the K_L decays to charged particles, and lower for events in which the K_L interacts in the calorimeter or escapes. This difference in trigger efficiency translates into the following values for the tag bias of the charged and neutral decay modes. From

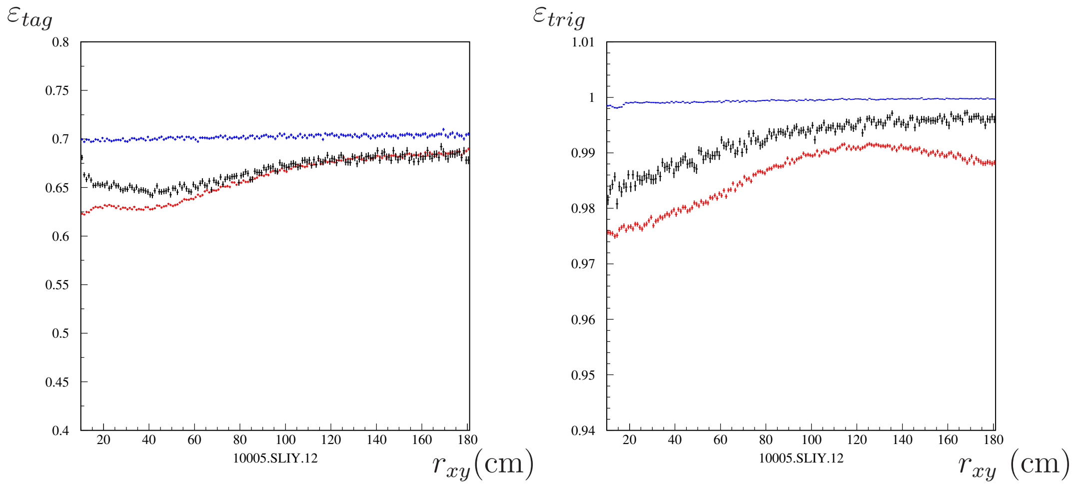

Fig. 1. Left: Tagging efficiency vs r_{xy}; Right: Trigger efficiency vs r_{xy} for tagged events. Different colors are used for different channels: blue for $\pi^0\pi^0\pi^0$, black for $\pi^+\pi^-$, red for $\pi^\pm\mu^\mp\nu$

Monte Carlo studies, we evaluate a tag bias value of about 0.99 and 1.06 for K_L decays to charged particles and to $3\pi^0$, respectively. As the ratio $\varepsilon_{\mathrm{tag}_{\pi^+\pi^-}}/\varepsilon_{\mathrm{tag}_{\pi\mu\nu}}$ is 1.0127, the measurement of the ratio of the BR's allows a partial cancellation of the tag bias contributions.

Moreover, the present accuracy of about 30% on the K_L-nuclear interaction cross section would translate into an uncertainty of about 3% in the absolute branching ratio measurement if it were necessary to obtain the absolute values of the trigger efficiencies from the Monte Carlo. Measuring the ratio of the BR's, the uncertainty on the K_L's nuclear interactions does not contribute.

The difference in the tagging efficiency also depends on the position of the K_L decay vertex. Fig. 1, left, shows the tagging efficiency as function of the transverse radial position of the K_L decay vertex for $\pi^0\pi^0\pi^0$,, $\pi^+\pi^-$and $\pi\mu\nu$.

The variation of the trigger efficiency as a function of the transverse radial position of the K_L decay vertex is shown in Fig. 1, right, for the $\pi^0\pi^0\pi^0$, $\pi^+\pi^-$and $\pi\mu\nu$ decay modes. This effect is mainly due to the use of position-dependent trigger thresholds.
Another contribution to the tag bias is the dependence of the reconstruction efficiency for the pion tracks from $K_S \to \pi^+\pi^-$ on the presence of other tracks in the drift chamber. This effect will be referred as *tracking interference*. It produces a difference in the tagging efficiencies for events with K_L decays to charged particles and to $3\pi^0$; this contribution to the tag bias additionally depends on the position of the K_L decay point (Fig. 1, left) .
As the $K_L \to \pi^+\pi^-$ and $K_L \to \pi\mu\nu$ contain both two charged particles, the effect of the tracking interference on them is similar and partially is canceled out

in the evaluation of $\varepsilon_{\text{tag},\,\pi^+\pi^-}/\varepsilon_{\text{tag}\,\pi\mu\nu}$.

The requirement that the trigger is produced by the K_S can reduce the difference on the trigger efficiencies among the K_L decays as well as the dependence of the tagging efficiency on the K_L decay position (Fig. 2, upper three curves). To identify events in which the K_S alone satisfies the calorimeter trigger, a minimal requirement is the presence of two clusters from the $K_S \to \pi^+\pi^-$ decay associated with fired trigger sectors. This kind of tag will be referred as second tag in the following. The resulting overall tagging efficiency is about 40% (without this further requirement the overall tagging efficiency is about 65%) but the difference between the tag bias values among the various channels is reduced: the average value of the tag bias for decays to charged particles is 0.98 and that for the $3\pi^0$ mode is 1.02. The ratio $\varepsilon_{\text{tag}_{\pi^+\pi^-}}/\varepsilon_{\text{tag}_{\pi\mu\nu}}$ is 1.0036.

The tracking interference effect is smaller when the pions from K_S decay are emitted orthogonally to the K_S direction. A cut on the difference of the pion momenta, $|\Delta P_{track}| < 60$ MeV, further reduces the difference in the tag bias values. This tag will be referred as third tag.
As a result, the efficiency of the tag is about 24% (Fig. 2, lower three curves), the tag bias for K_L decays to charged particles is about 0.97 and that for decays to $3\pi^0$ is about 1.00. The ratio $\varepsilon_{\text{tag}_{\pi^+\pi^-}}/\varepsilon_{\text{tag}_{\pi\mu\nu}}$ is 0.9968.

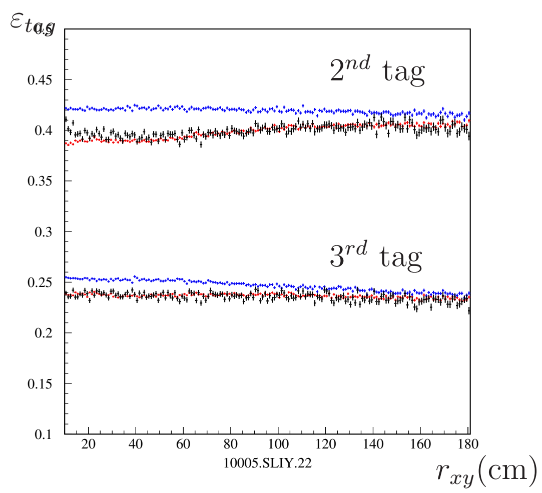

Fig. 2. Tagging efficiency vs r_{xy} obtained using two different tagging criteria. Different colors are used for different channels: blue for $\pi^0\pi^0\pi^0$, black for $\pi^+\pi^-$, red for $\pi^\pm\mu^\mp\nu$

In this analysis the standard tag is used. The requirement of a self-triggering tag (second tag) would decrease the statistics (BR($K_L \to \pi^+\pi^-$) $\sim 2 \times 10^{-3}$). From MC studies the use of the second or third tag reduces the systematic error in the measurement, but would not compensate the corresponding increase of the statistical error. Therefore the second and third tag are used to study and to evaluate the systematic error due to the tag efficiency evaluation (Sec. 7.1).

3 Extrapolation of tracks from K_L decay

All tracks in the chamber, after removal of those from the K_S decay and their descendants, are extrapolated to their points of closest approach to the *tagging line*. For each candidate track the point $\mathbf{x}_\mathrm{c}$ of closest approach to the K_L line of flight is analytically extrapolated. At $\mathbf{x}_\mathrm{c}$ the distance of closest approach, d_c, the momentum $\mathbf{p}_\mathrm{c}$ of the track at $\mathbf{x}_\mathrm{c}$ and the extrapolation length, l_c, from the first track hit are calculated. l_c is defined positive if $\mathbf{x}_\mathrm{c}$ is after the first track hit along the K_L line of flight, negative in the other case. Tracks satisfying $d_\mathrm{c} < a r_{xy} + b$, with $a = 0.03$ and $b = 3$ cm, and -20 cm $< l_\mathrm{c} <$ 25 cm are accepted as K_L decay products, being r_{xy} the distance of the vertex from the IP in the transverse plane. For each sign of charge we consider as associated to the K_L decay the track with the smallest value of d_c. Starting from these track candidates a vertex is reconstructed. The events are retained if the vertex is in the fiducial volume $30 < r_{xy} < 150$ cm and $|z| < 120$ cm. Measured momenta on MC events have been smeared as described in Ref. 6 to improve the agreement with data.

4 Choice of the fiducial volume

The fiducial volume has been defined in a region of stability of the result. Instability can arise both on the tag bias evaluation and on the reconstruction efficiency evaluation.

In Sec. 2 is pointed out that the tag bias depends on the position of the K_L decay vertex (Fig. 1). Also the reconstruction efficiency depends on the K_L decay vertex, as can be seen by comparing the r_{xy} distributions for $K_L \to \pi^+\pi^-$and for $K_L \to \pi\mu\nu$ MC events satisfying the second tag in Fig. 3, left. Therefore, in order to study the impact of the data-MC discrepancy on the results and to choose the proper fiducial volume, the variation of the result by varying the fiducial volume has been studied.
The fiducial volume has been enlarged in step of 5 cm from the lower limit (30 cm) up to the upper limit (150 cm). Hence, 23 fiducial volumes are defined and at each step the fiducial region is enlarged:

$$\mathrm{FV}_1 : 30 < r_{xy} < 35\,\mathrm{cm}$$

$$\mathrm{FV}_2 : 30 < r_{xy} < 40\,\mathrm{cm}$$

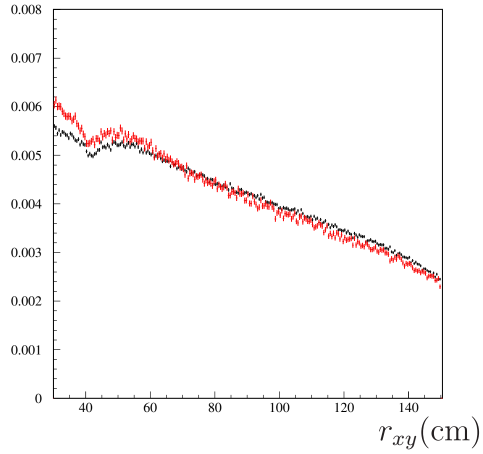

Fig. 3. Left: r_{xy} distributions for $K_L \to \pi^+\pi^-$ (red points) and for $K_L \to \pi\mu\nu$ (black points) MC events . Both distributions are normalized to one.

$$\mathrm{FV}_3 : 30 < r_{xy} < 45\,\mathrm{cm}...$$

In each step the number of $K_L \to \pi^+\pi^-$ events, $N_{\pi^+\pi^-}$, and of $K_L \to \pi\mu\nu$ events, $N_{\pi\mu\nu}$, have been obtained from the data through the fit of the $\Delta_{\mu\pi}$ and $\sqrt{E^2_{miss} + p^2_{miss}}$ distributions respectively, as will be explained in Sec. 6. From the MC the number of $K_L \to \pi^+\pi^-$ events, $N^{MC}_{\pi^+\pi^-}$, and $K_L \to \pi\mu\nu$ events, $N^{MC}_{\pi\mu\nu}$, are also evaluated for each step.

These latter have been corrected for the tracking efficiency (as explained in Sec. 5.2).

In each step the double ratio $R^{\mathrm{up}} = \frac{N_{\pi^+\pi^-}}{N_{\pi\mu\nu}} / \frac{N^{MC}_{\pi^+\pi^-}}{N^{MC}_{\pi\mu\nu}}$ is obtained.

The same procedure has been done by starting from the upper limit of the FV:

$$\mathrm{FV}_1 : 145 < r_{xy} < 150\,\mathrm{cm}$$

$$\mathrm{FV}_2 : 140 < r_{xy} < 150\,\mathrm{cm}$$

$$\mathrm{FV}_3 : 135 < r_{xy} < 150\,\mathrm{cm}...$$

and for each step the double ratio $R^{\mathrm{down}} = \frac{N_{\pi^+\pi^-}}{N_{\pi\mu\nu}} / \frac{N^{MC}_{\pi^+\pi^-}}{N^{MC}_{\pi\mu\nu}}$ is obtained. The distributions of R^{up} and R^{down} have been normalized in a region of stability (130 cm for R^{up} and 45 cm for R^{down}) and are subtracted from one. They are shown in Fig. 4: the red (black) points correspond to the R^{up} (R^{down}) distribution. Only the statistical relevant points of the distribution,*i.e.* the first points R^{up} and the last of R^{down}, are shown. The errors shown are correlated because the correspondent samples are not independent.

The distributions R^{up} and R^{down} can be compared with the relative statistical

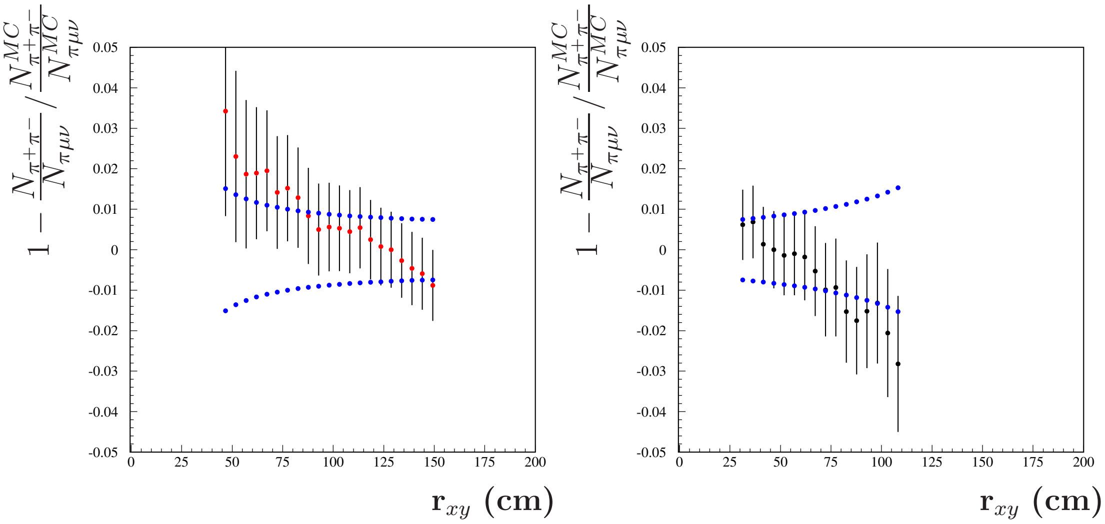

Fig. 4. Distribution of $1 - \frac{N_{\pi^+\pi^-}}{N_{\pi\mu\nu}}/\frac{N^{MC}_{\pi^+\pi^-}}{N^{MC}_{\pi\mu\nu}}$ as a function of the increasing size of the fiducial volume, enlarged from r_{xy} =30 cm up to 150 cm (uppper plot, red points) and from r_{xy} =150 cm down to 30 cm (lower plot, black points). For both distributions the errors shown are correlated, because the samples corresponding to increasing size of the fiducial volume are not independent. Points at low (high) r_{xy} of the upper (lower) plot are omitted because of the limited statistics. The blue points are the edges of the correspondent statistical errors.

error $\Delta_{\rm stat} = \sqrt{\left(\frac{\Delta N_{\pi^+\pi^-}}{N_{\pi^+\pi^-}}\right)^2 + \left(\frac{\Delta N_{\pi\mu\nu}}{N_{\pi\mu\nu}}\right)^2}$. In Fig. 4 the dependence of the statistical error as a function of the increasing size of the fiducial volume is also shown: the upper limit of the FV has been *a posteriori* chosen as the intersection point (150 cm) between the statistical error and the $R^{\rm up}$ distribution. Analogously, the lower limit has been *a posteriori* chosen as the intersection point between the statistical error and the $R^{\rm dw}$ distribution (30 cm) (Fig. 4). Therefore, with this choice of the FV, the result is stable within the statistical error. It is worthwhile noting that this procedure takes into account every source of data-MC discrepancy that affect the r_{xy} distribution.

5 Efficiencies evaluation

5.1 Tagging efficiency

The tagging efficiency, $\varepsilon_{{\rm tag}\,k}$, has been evaluated from MC. The tagging procedure used to signal a K_L, described in details in Sec. 2, requires a $K_S \to \pi^+\pi^-$ decay selected with loose kinematical cuts and a cluster with energy greater than 50 MeV produced by a π from the K_S (which gives the t_0 of the event). The tagging efficiency for decays in $\pi^+\pi^-$ and for $\pi\mu\nu$, evaluated from MC for a single data period, are respectively :

$$\varepsilon_{\mathrm{tag}\,\pi^+\pi^-} = 0.66316 \pm 0.00045$$

$$\varepsilon_{\mathrm{tag}\,\pi\mu\nu} = 0.65483 \pm 0.00042$$

The systematic error due to the evaluation of the tagging efficiency is obtained in Sec. 7.1.

5.2 Reconstruction efficiency

The reconstruction efficiency for a decay $K_L \to k$ can be expressed as follows:

$$\varepsilon_{\mathrm{rec}\,k} = \frac{N_{\mathrm{rec}\,k}}{N_{\mathrm{tag}\,k}} \tag{3}$$

where the $N_{\mathrm{rec\,k}}$ is the number of K_L decays with two good tracks forming a vertex (Sec. 3) and $N_{\mathrm{tag\,k}}$ the number of K_L's tagged.

5.3 Reconstruction efficiency for single tracks

The reconstruction efficiency has been obtained from MC and has been corrected by evaluating the *conditional* efficiencies for data and MC. Both the reconstruction efficiency and the correction are run-period dependent. The conditional efficiency can be determined by counting the number of events in which there is a K_L decay track of at least one sign and the number of events in which there are two decay tracks of opposite sign:

$$\epsilon^{cond} = N_{2\,\mathrm{tracks}}/N_{1\,\mathrm{track}}.$$

The ratio between these efficiencies for data and for MC is then used to correct the MC estimate for the reconstruction efficiency.
This correction is evaluated as function of the track momentum using $K_L \to \pi^+\pi^-\pi^0$ and $K_L \to \pi^\pm e^\mp \nu$ events.

To select $K_L \to \pi^+\pi^-\pi^0$ events, at least one good K_L decay track and two photons from a π^0 decay are required. To reject background, cuts are applied on the two-photon invariant mass and on the times of flight of the photons. The selection is described in more details in Ref. 6. The momentum of one decay track is calculated from kinematics by using the two photons from the π^0 decay and the momentum of the other decay track. The resolution obtained is about 10 MeV.

In order to obtain corrections for higher momenta tracks (above 150 MeV), $\pi^\pm e^\mp \bar{\nu}_e(\nu_e)$ decays are used. $K_L \to \pi^\pm e^\mp \bar{\nu}_e(\nu_e)$ are selected by identifying the

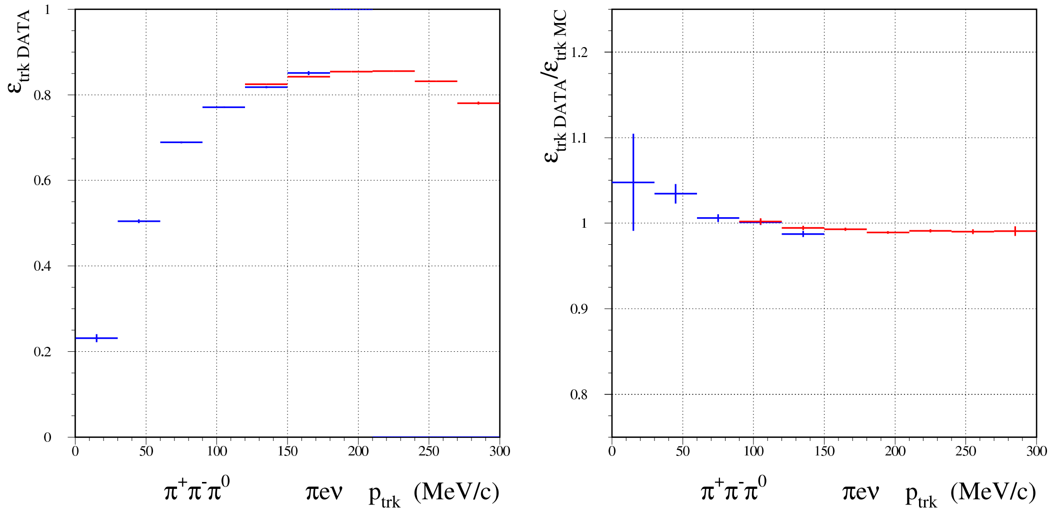

Fig. 5. Left: Conditional tracking efficiency from $K_L \rightarrow \pi^+\pi^-\pi^0$ (blue) and $K_L \rightarrow \pi^\pm e^\mp \bar{\nu}_e(\nu_e)$ (red) events, for data for a single run period. Right: Data-Monte Carlo ratio of conditional tracking efficiencies for the two samples for a single run period.

electrons by time of flight with a purity of 95%. The remaining background is due mostly to $K_{\mu 3}$ decays. The details of the selection can be found in Ref. 6. The momentum of the second K_L track is evaluated from the missing energy with a resolution of 30 MeV.

The comparison of the efficiencies obtained with $K_L \rightarrow \pi^\pm e^\mp \bar{\nu}_e(\nu_e)$ events and $K_L \rightarrow \pi^+\pi^-\pi^0$ events shows good agreement in the overlap region 100–150 MeV (Fig. 5). In the region below 100 MeV, the conditional tracking efficiency from $K_L \rightarrow \pi^\pm e^\mp \bar{\nu}_e(\nu_e)$ events is systematically bigger than that from $K_L \rightarrow \pi^+\pi^-\pi^0$ events. This effect is due both to the differences in the selection criteria and to the worse resolution in the expected track momentum in $K_L \rightarrow \pi^\pm e^\mp \bar{\nu}_e(\nu_e)$ events at small expected momentum. In particular, due to the resolution effect, contributions from high momenta particles in the bins of low momentum values increase systematically the efficiency. As the expected momentum is determined with better precision in $K_L \rightarrow \pi^+\pi^-\pi^0$ events at low momentum, for momenta smaller than 150 MeV, the correction obtained from this sample is used, while for momenta greater than 150 MeV, the correction obtained from $K_L \rightarrow \pi^\pm e^\mp \bar{\nu}_e(\nu_e)$ events is used.
Finally, the correction is calculated as

$$f_{\mathrm{trk\,corr}}(\mathbf{p}_{\mathrm{trk}}) = \varepsilon_{\mathrm{data}}/\varepsilon_{\mathrm{MC}} \tag{4}$$

and is applied period by period as a function of momentum in 30 MeV bins. It is shown in Fig. 6, right, for a single run period.

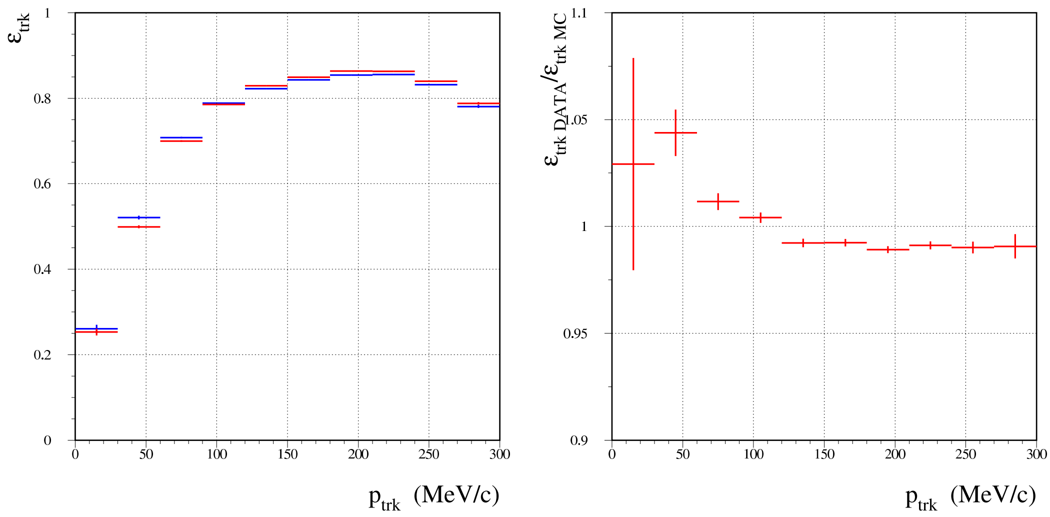

Fig. 6. Left: Conditional tracking efficiency estimated using $K_L \rightarrow \pi^+\pi^-\pi^0$ and $K_L \rightarrow \pi^\pm e^\mp \bar{\nu}_e(\nu_e)$ decays, as a function of expected track momentum, for Monte Carlo (red) and data (blue) for a single run period. Right: Data-Monte Carlo ratio of conditional tracking efficiencies for a single run period.

5.4 Reconstruction efficiency for events with two tracks

As the $K_L \rightarrow \pi^+\pi^-$ and $K_L \rightarrow \pi\mu\nu$ decays contain two charged tracks, the correction to the *single* track reconstruction efficiency (4) cannot be directly used. The correction should moreover be applied to the *ratio* of the reconstruction efficiencies $\varepsilon_{\text{rec}\,\pi^+\pi^-}/\varepsilon_{\text{rec}\,\pi\mu\nu}$ in (2) and should be averaged on particles momenta.
For this purpose, MC techniques have been exploited and one hundred of samplings of the correction:

$$\text{corr}(\mathbf{p}^i_{\text{trk}}, k) = f_{\text{trk corr}}(\mathbf{p}^i_{\text{trk}}) + ran(k) \cdot \Delta f_{\text{trk corr}\,i}(\mathbf{p}^i_{\text{trk}})$$

have been constructed, where i is + (-) for the positive (negative) track, $f_{\text{trk corr}}(\mathbf{p}_{\text{trk}})$ is the correction shown in Fig. 6, ran(k) is a random number with normalized gaussian distribution, k is the sampling number and $\Delta f_{\text{trk corr}}(\mathbf{p}_{\text{trk}})$ is the error associated to the correction.
Then, for each decay channel in MC events, the average, $\text{corr}_\pm(k)$, on the momenta of the product of the corrections,

$$\text{corr}_\pm(k) = \left\langle \text{corr}(\mathbf{p}^+_{\text{trk}}, k) \ \cdot \ \text{corr}(\mathbf{p}^-_{\text{trk}}, k) \right\rangle ,$$

has been obtained and used to evaluate the correction associated to the sampling k. Then, the ratio of the average corrections for $\pi^+\pi^-$ and $\pi\mu\nu$ events, $\text{corr}_{\pm\,\pi^+\pi^-}(k)/\text{corr}_{\pm\,\pi\mu\nu}(k)$, shown in Fig. 7 for a single run period, is calculated. The average of the ratios of the corrections for $\pi^+\pi^-$and $\pi\mu\nu$ events, $\text{corr}_{\pm\,\pi^+\pi^-}/\text{corr}_{\pm\,\pi\mu\nu}$, on the samplings is then used to correct the MC estimates for the reconstruction efficiencies as follows:

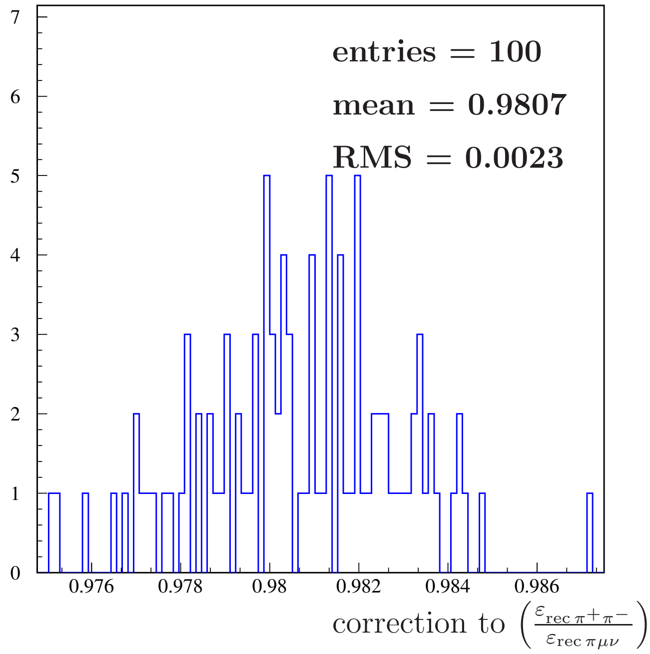

Fig. 7. Distribution of the ratio of the corrections for $\pi^+\pi^-$and $\pi\mu\nu$ events for a single run period.

$$\left(\frac{\varepsilon_{\mathrm{rec}\,\pi^+\pi^-}}{\varepsilon_{\mathrm{rec}\,\pi\mu\nu}}\right)_{\mathrm{corr}} = \left(\frac{\varepsilon_{\mathrm{rec}\,\pi^+\pi^-}}{\varepsilon_{\mathrm{rec}\,\pi\mu\nu}}\right)_{\mathrm{MC}} \cdot \left\langle \frac{\mathrm{corr}_{\pm\,\pi^+\pi^-}}{\mathrm{corr}_{\pm\,\pi\mu\nu}} \right\rangle$$

The RMS of the $\mathrm{corr}_{\pm\,\pi^+\pi^-}/\mathrm{corr}_{\pm\,\pi\mu\nu}$ distribution is used to evaluate the statistical error on the correction, whose contribution to the total relative statistical error is:

$$\delta_{\mathrm{corr}} = \frac{\mathrm{RMS}\left(\frac{\mathrm{corr}_{\pm\,\pi^+\pi^-}}{\mathrm{corr}_{\pm\,\pi\mu\nu}}\right)}{\left\langle \frac{\mathrm{corr}_{\pm\,\pi^+\pi^-}}{\mathrm{corr}_{\pm\,\pi\mu\nu}} \right\rangle}$$

6 Counting

Monte Carlo studies have shown that the best discriminant amongst the main K_L decay modes into charged particles is the smaller of the two possible values of $\Delta_{\mu\pi}=|\mathbf{p}_{\rm miss}|-E_{\rm miss}$, where $\mathbf{p}_{\rm miss}$ and $E_{\rm miss}$ are the missing momentum and energy at the K_L vertex, evaluated by assigning to one track the pion mass and to the other one the muon mass. The shape of the $\Delta_{\mu\pi}$ spectrum is very sensitive to the radiative corrections to K_L decay processes. The KLOE Monte Carlo includes very accurate generators for the radiative channels, as described in Ref. 11. The measurement here presented is therefore fully inclusive with respect to final state radiation.
The number of $K_L \to \pi^\pm\mu^\mp\nu(\gamma)$ are obtained from fits to the $|\mathbf{p}_{\rm miss}| - E_{\rm miss}$ distributions with a linear combination of MC distributions. The result of the fit for a single run period is shown in Fig. 8. From MC studies the best variable to

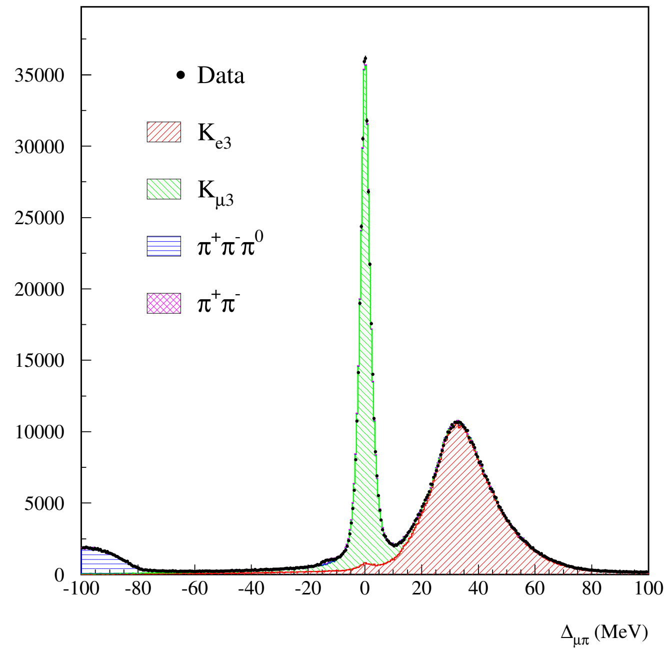

Fig. 8. Distribution of $\Delta_{\mu\pi}$for a single run period, with fit to MC distributions for different decay channels

select $K_L \to \pi^+\pi^-(\gamma)$ is $\sqrt{E^2_{miss} + |\mathbf{p}_{miss}|^2}$ where

- $\mathbf{p}_{miss}$ is the difference between the K_L momentum (resulting from the tagging procedure, Sec. 2) and sum of the momenta of particle coming from the K_L decay

$$\mathbf{p}_{miss} = \mathbf{p}_{K_L} - (\mathbf{p}_1 + \mathbf{p}_2)$$

- E_{miss} is the missing energy in the hypothesis of $K_L \rightarrow \pi^+\pi^-$ decay

$$E_{miss} = E_{K_L} - \sqrt{|\mathbf{p}_1|^2 + m_\pi^2} - \sqrt{|\mathbf{p}_2|^2 + m_\pi^2}$$

The result of the fit for a single run period is shown in Fig. 9. The signal region is shown in Fig. 10

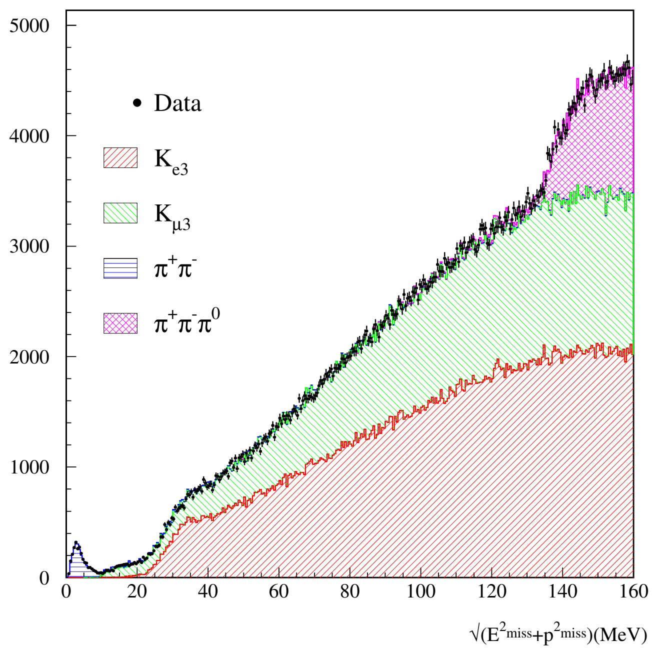

Fig. 9. Distribution of $\sqrt{E_{miss}^2 + |\mathbf{p}_{miss}|^2}$ for a single run period, with fit to MC distributions for different decay channels

For each run period the ratio of the number of $K_L \rightarrow \pi^+\pi^-$ and $K_L \rightarrow \pi\mu\nu$ events is obtained : $N_{\pi^+\pi^-}/N_{\pi\mu\nu}$, where $N_{\pi^+\pi^-}$ is the number of $K_L \rightarrow \pi^+\pi^-$ events as resulting from the fit of the $\sqrt{E_{miss}^2 + |\mathbf{p}_{miss}|^2}$ distribution, while $N_{\pi\mu\nu}$ is the number of $K_L \rightarrow \pi\mu\nu$ events as resulting from the fit of the $|\mathbf{p}_{\text{miss}}| - E_{\text{miss}}$ distribution

7 Systematics

The systematic errors due to the finite statistics in the evaluation of the corrections, data-MC inconsistency and instabilities of the signal extraction have been studied. Correlation with the others KLOE BR's results used for the normalization has been taken into account.

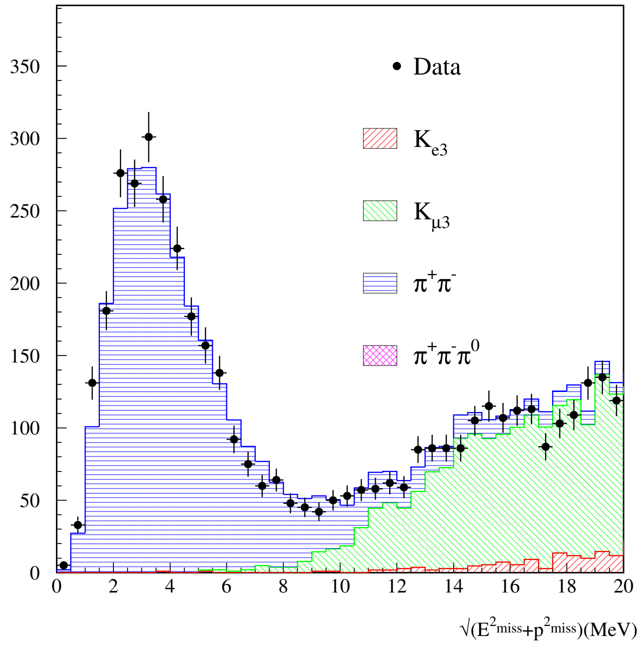

Fig. 10. Distribution of $\sqrt{E^2_{miss} + |\mathbf{p}_{miss}|^2}$ for a single run period, with fit to MC distributions for different decay channels

7.1 Tagging efficiency

The systematic error on the evaluation of the ratio of the tagging efficiencies

$$\varepsilon_{\mathrm{tag}\,\pi^+\pi^-}/\varepsilon_{\mathrm{tag}\,\pi\mu\nu},$$

has been evaluated from the study of the stability of the results obtained with different tagging criteria. Two other tags have been defined as explained above. In Fig. 11 the results of the BR($K_L \to \pi^+\pi^-$)/BR($K_L \to \pi\mu\nu$) for different data periods obtained using different tags are shown. Since the samples are not independent, the statistical error shown in Fig. 11 are correlated.

- first tag: $(0.7244 \pm 0.0042) \times 10^{-2}$ with $\chi^2/\mathrm{dof} = 9.0452/13$
  $\bar{\varepsilon}_{\mathrm{tag}} \simeq 65\%$
- second tag: $(0.7268 \pm 0.0056) \times 10^{-2}$ with $\chi^2/\mathrm{dof} = 11.18/13$
  $\bar{\varepsilon}_{\mathrm{tag}} \simeq 40\%$
- third tag: $(0.7253 \pm 0.0072) \times 10^{-2}$ with $\chi^2/\mathrm{dof} = 12.96/13$
  $\bar{\varepsilon}_{\mathrm{tag}} \simeq 24\%$.

A conservative evaluation of the systematic error due to the tagging efficiency evaluation is the largest difference among the results obtained with different tags:

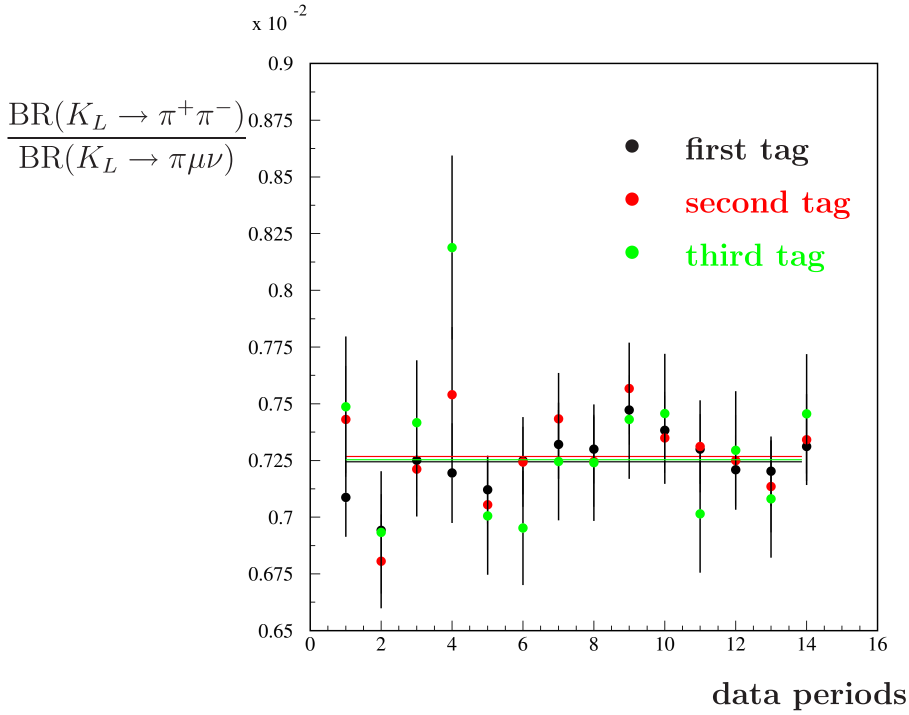

Fig. 11. Results of $\mathrm{BR}(K_L \to \pi^+\pi^-)/\mathrm{BR}(K_L \to \pi\mu\nu)$ for different data periods obtained using different tags. Only statistical errors are shown.

$$\Delta_{\mathrm{tgb,\,syst}} = \left(\frac{\mathrm{BR}(K_L \to \pi^+\pi^-)}{\mathrm{BR}(K_L \to \pi\mu\nu)}\right)_{2^{\mathrm{nd}}\,\mathrm{tag}} - \left(\frac{\mathrm{BR}(K_L \to \pi^+\pi^-)}{\mathrm{BR}(K_L \to \pi\mu\nu)}\right)_{1^{\mathrm{th}}\,\mathrm{tag}} =$$
$$= 0.0023 \times 10^{-2}$$

7.2 Tracking efficiency

The same method of Ref. 6 has been used to evaluate the systematic uncertainty on the tracking efficiency. The uncertainty of the tracking efficiency correction is dominated by the sample statistics and by the variation of the results observed by using different criteria to identify good tracks from the K_L decays.

The correction of the tracking efficiency (Sec. 5.3) is run-period dependent: its statistical error is added in quadrature for each period to the other statistic errors (Sec. 8).

The systematic error due to the definition of good tracks coming from the K_L decay is obtained by varying the cuts on the variables used to associate tracks to K_L vertices (Sec. 3). In particular, the cut on d_c has been changed: the value of b has been varied from 1 cm to 5 cm and the cut on l_c has been varied from 15 cm to 35 cm. For each configuration the complete tracking efficiency correction has been obtained. In Table 1 the relative variations of the tracking efficiency and of the ratio R = BR($K_L \to \pi^+\pi^-$)/BR($K_L \to \pi\mu\nu$) with respect to the cut applied in the analysis (Sec. 3) are summarized. The systematic error on

	d_c **cut (cm),** l_c **cut (cm)**			
	1, 25	5, 25	3, 15	3, 35
$\delta\varepsilon_{\mathrm{rec},\pi^+\pi^-}$	0.083	-0.026	0.0613	-0.32
$\delta\varepsilon_{\mathrm{rec},\pi\mu\nu}$	0.10	-0.033	0.068	-0.037
δ R	-0.0031	0.0039	-0.0048	-0.0048

Table 1
Relative variations of the tracking efficiency ($\delta\varepsilon = \frac{\Delta\varepsilon}{\varepsilon}$) and of the ratio R = BR($K_L \to \pi^+\pi^-$)/BR($K_L \to \pi\mu\nu$) ($\delta R = \frac{\Delta R}{R}$) with respect to the cut applied in the analysis

the tracking efficiency evaluation is taken as the RMS of the results obtained with these five different track definitions (including the one used in the analysis): $\Delta_{\mathrm{rec,syst}} = 0.0027 \times 10^{-2}$.
Since the method used to evaluate the error on the tracking efficiency is the same as the one used for the K_L's main BR's analysis [12], we evaluate the correlations between the K_L's main BR's and the BR($K_L \to \pi^+\pi^-$) which will be used in the following (Sec. 8). The error matrix for the tracking efficiency in Table 2 shows the covariance $\langle\sigma_i\sigma_j\rangle$ (i, j are the decay channels) obtained varying the track definitions as explained above.

	$\pi^+\pi^-$- $\pi^\pm e^\mp\nu$	$\pi^+\pi^-$-$\pi^\pm\mu^\mp\nu$	$\pi^+\pi^-$-$\pi^+\pi^-\pi^0$	$\pi^+\pi^-$-$\pi^+\pi^-$
$\langle\sigma_i\sigma_j\rangle$	7.43 $\times10^{-9}$	5.57 $\times10^{-9}$	4.25 $\times10^{-9}$	0.74$\times10^{-9}$

Table 2
Tracking uncertainty error matrix row

7.3 Signal extraction

The systematic error due to the reliability of the Monte Carlo distributions on the variables $|\mathbf{p}_{\mathrm{miss}}| - E_{\mathrm{miss}}$ and $\sqrt{E_{miss}^2 + p_{miss}^2}$ has been evaluated by studying the sensitivity of R to the momentum resolution. A different approach has been used with respect to Ref. 6 due to the limited amount of statistics. The fit to the $\sqrt{E_{miss}^2 + p_{miss}^2}$ and the $|\mathbf{p}_{\mathrm{miss}}| - E_{\mathrm{miss}}$ distribution has been repeated using Monte Carlo samples in which the momentum resolutions has been varied according to the uncertainty. As described in Ref. 6 the momentum resolution has a narrow gaussian large component(core) and a wider gaussian small component(tail). The uncertainties on the momentum resolution parameters has been evaluated in a different way for the core and the tail. The fit to the $\sqrt{E_{miss}^2 + p_{miss}^2}$ and $|\mathbf{p}_{\mathrm{miss}}| - E_{\mathrm{miss}}$ distribution has been repeated using Monte Carlo samples in which the parameters describing the core of the momentum resolutions have been varied.

This variation results in a worsening of the fit quality: a decrease of the χ^2 fit probability of $\pm$ 1 σ corresponds to a fractional variation of $\delta_{\text{shape,R}} = 0.0022$.

A different method has been used for the evaluation of the uncertainties on the parameters used to describe the tail. They have been evaluated comparing the data and Monte Carlo $|\mathbf{p}_{\text{miss}}| - E_{\text{miss}}$ distributions on the K_{e3} and $K_{\mu 3}$ control samples selected with calorimeter informations as described in Ref. 6. A fractional variation of $\delta_{\text{shape,R}} = 0.0050$ has been found.

8 Results

The final result has been calculated as the mean over the 14 periods of data taking.

Different sources contributes to the total statistical error in each period:

- the counting of $K_L \to \pi^+\pi^-$ and $K_L \to \pi\mu\nu$ events, whose contribution to the relative uncertainty is given by:

$$\delta_{cnt} = \sqrt{\left(\frac{\Delta N_{\pi^+\pi^-}}{N_{\pi^+\pi^-}}\right)^2 + \left(\frac{\Delta N_{\pi\mu\nu}}{N_{\pi\mu\nu}}\right)^2}$$

- the evaluation of the tag bias, which contributes with the following relative error:

$$\delta_{tgb} = \sqrt{\left(\frac{\Delta_{tgb_{\pi^+\pi^-}}}{\varepsilon_{\text{tag}_{\pi^+\pi^-}}/\varepsilon_{\text{tag}_{\text{tot}}}}\right)^2 + \left(\frac{\Delta_{tgb_{\pi\mu\nu}}}{\varepsilon_{\text{tag}_{\pi\mu\nu}}/\varepsilon_{\text{tag}_{\text{tot}}}}\right)^2}$$

- the reconstruction efficiency, which contributes with the following relative error:

$$\delta_{rec} = \sqrt{\left(\frac{\Delta\varepsilon_{\text{rec}\pi^+\pi^-}}{\varepsilon_{\text{rec}\pi^+\pi^-}}\right)^2 + \left(\frac{\Delta\varepsilon_{\text{rec}\pi\mu\nu}}{\varepsilon_{\text{rec}\pi\mu\nu}}\right)^2}$$

- the tracking efficiency correction, whose error is related to the RMS of the correction distribution, as explained in Sec. 5.4

$$\delta_{\text{corr}} = \frac{\text{RMS}\left(\dfrac{\text{corr}_{\pm\,\pi^+\pi^-}}{\text{corr}_{\pm\,\pi\mu\nu}}\right)}{\left\langle\dfrac{\text{corr}_{\pm\,\pi^+\pi^-}}{\text{corr}_{\pm\,\pi\mu\nu}}\right\rangle}$$

The statistical error for each period is therefore given by:

$$\Delta_{stat} = \frac{BR(K_L \to \pi^+\pi^-)}{BR(K_L \to \pi\mu\nu)} \cdot \sqrt{\delta^2_{cnt} + \delta^2_{tgb} + \delta^2_{rec} + \delta^2_{corr}} \qquad (5)$$

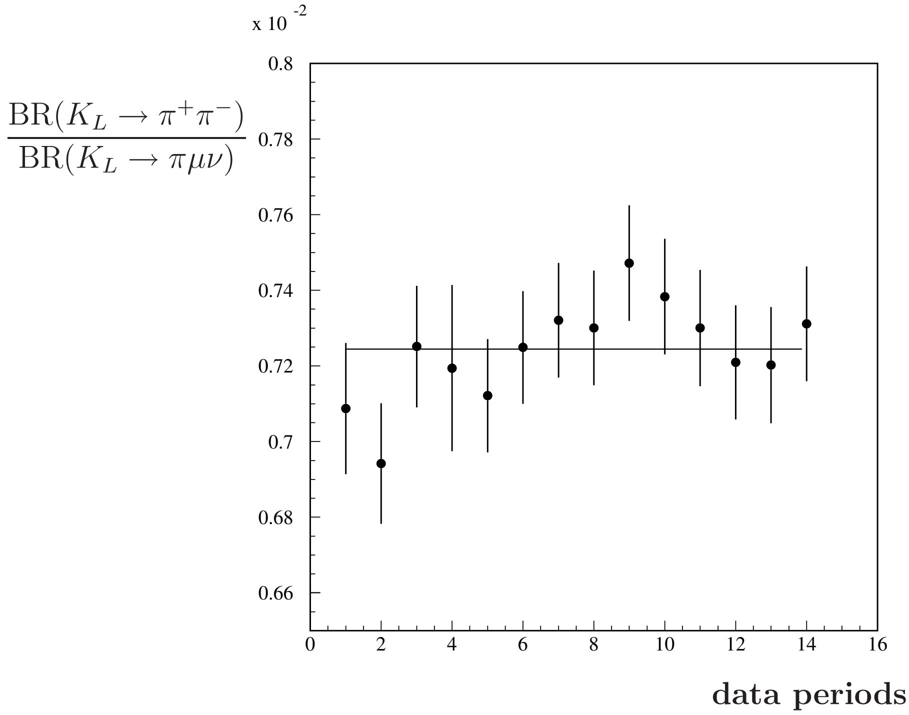

Fig. 12. Results of $\mathrm{BR}(K_L \to \pi^+\pi^-)/\mathrm{BR}(K_L \to \pi\mu\nu)$ for different data periods. Only statistical errors are shown.

The good stability of the results can be seen in Fig. 12 in which only the statistical errors are reported. The result of the fit is $(0.7245 \pm 0.0042) \times 10^{-2}$ with $\chi^2/\mathrm{dof} = 9.045/13$.

Finally, the results on the ratio $\mathrm{R}{=}\mathrm{BR}(K_L \to \pi^+\pi^-)/\mathrm{BR}(K_L \to \pi\mu\nu)$ is:

$$(0.7275 \pm 0.0042_{\mathrm{stat}} \pm 0.0027_{\mathrm{track,syst}} \pm 0.0023_{\mathrm{tag,syst}} \pm 0.0040_{\mathrm{shape}}) \times 10^{-2}$$

where

- the "stat" error includes the statistical errors due to the counting, the reconstruction efficiency, the correction and the tag bias,
- the "track" error is the systematic error on the tracking efficiency.
- the "tag" error is the systematic error due to the tag bias evaluation,
- the "shape" error is due to the reliability of the MC distributions on the variables $|\mathbf{p}_{\mathrm{miss}}| - E_{\mathrm{miss}}$ and $\sqrt{E^2_{miss} + p^2_{miss}}$ used to count the $K_L \to \pi^+\pi^-$ and $K_L \to \pi\mu\nu$ events,

Using the KLOE result for $\mathrm{BR}(K_L \to \pi\mu\nu)$ and the correlations with the main K_L BR's (App. A), we found:

$$\mathrm{BR}(K_L \to \pi^+\pi^-) = (1.963 \pm 0.012_{\mathrm{stat.}} \pm 0.017_{\mathrm{syst.}}) \times 10^{-3}$$

The error on the measurement of $\mathrm{BR}(K_L \to \pi\mu\nu)$ of Ref. 6 is correlated with the errors on $\mathrm{BR}(K_L \to \pi e\nu)$, $\mathrm{BR}(K_L \to \pi^0\pi^0\pi^0)$, $\mathrm{BR}(K_L \to \pi^+\pi^-\pi^0)$, and the K_L lifetime. This is because, in the treatment of Ref. 6, the branching ratios and the lifetime are determined from lifetime-dependent absolute branching ratio measurements using the constraint $\sum \mathrm{BR} = 1 - 0.0036$, where 0.0036 represents the small contribution due to the sum of the branching ratios for $K_L \to \pi^+\pi^-$, $K_L \to \pi^0\pi^0$, and $K_L \to \gamma\gamma$ listed in the PDG compilation [3]. As a consequence, the error on the value for $\mathrm{BR}(K_L \to \pi^+\pi^-)$ reported here is correlated with the errors on the branching ratio and K_L lifetime values reported in Ref. 6. Additional sources of correlation arise from common systematic uncertainties in the tracking efficiency evaluation (Table 2).

The complete correlation matrix is:

$$\begin{pmatrix} 1 & -0.25 & -0.56 & -0.07 & -0.12 & 0.25 \\ & 1 & -0.43 & -0.20 & 0.51 & 0.33 \\ & & 1 & -0.39 & -0.24 & -0.21 \\ & & & 1 & -0.09 & -0.39 \\ & & & & 1 & 0.11 \\ & & & & & 1 \end{pmatrix}$$

where the columns and the rows refer, in order, to the BR's for decays to $\pi^\pm e^\mp\nu$, $\pi^\pm\mu^\mp\nu$, $\pi^0\pi^0\pi^0$, $\pi^+\pi^-\pi^0$ and $\pi^+\pi^-$, and τ_{K_L}. Because $\mathrm{BR}(K_L \to \pi^+\pi^-)$ is small, the KLOE values for the dominant BR's are essentially unchanged when the new KLOE value for $\mathrm{BR}(K_L \to \pi^+\pi^-)$ is used in constraining the sum of the K_L BR's to unity.

Adding the statistical and systematic errors in quadrature, we get:

$$\mathrm{BR}(K_L \to \pi^+\pi^-) = (1.963 \pm 0.021) \times 10^{-3}$$

The result is in good agreement with the one obtained by KTeV [2]:

$$(1.975 \pm 0.012) \times 10^{-3}.$$

Our value for the $\mathrm{BR}(K_L \to \pi^+\pi^-)$ is in strong disagreement with that reported by the PDG, $(2.090 \pm 0.025) \times 10^{-3}$ [3]: A difference of 5% corresponding to $\sim$4 standard deviations is observed. The measurements are shown in Fig. 13.

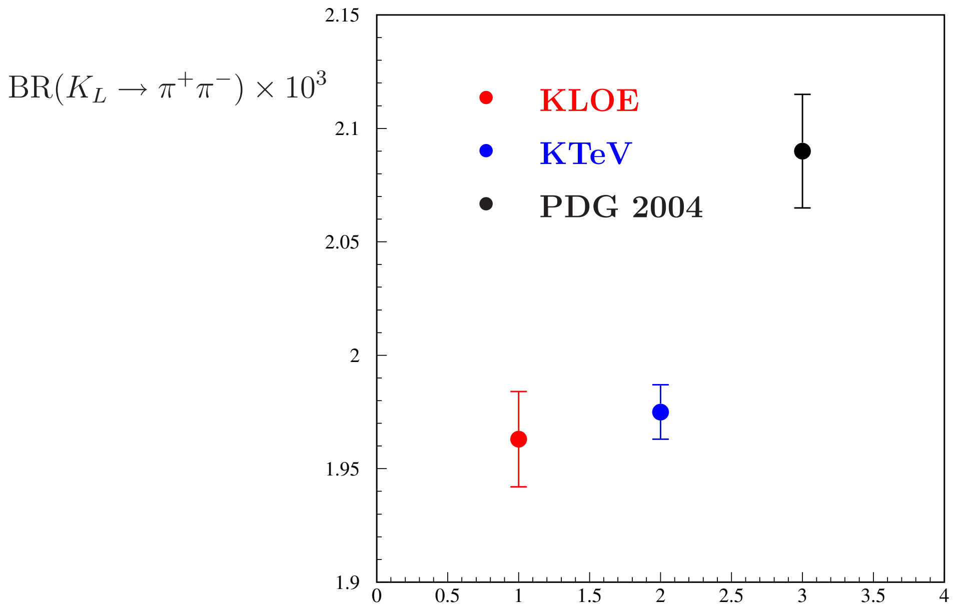

Fig. 13. Results of $BR(K_L \to \pi^+\pi^-)$ of KLOE, KTeV and PDG 2004

9 Extraction of $|\epsilon|$ and impact on the Unitarity Triangle

The measurement of $BR(K_L \to \pi^+\pi^-)$ can be used to determine $|\epsilon|$ through

$$\eta_\pm = \epsilon + \epsilon' \tag{6}$$

$$|\eta_\pm| = \sqrt{\frac{\Gamma(K_L \to \pi^+\pi^-)}{\Gamma(K_S \to \pi^+\pi^-)}} \tag{7}$$

correcting for the small contribution of ϵ'. Using the measurements of $BR(K_S \to \pi^+\pi^-)$ and τ_{K_L} from KLOE [13] [6], and the value of τ_{K_S} from PDG [3], and subtracting the contribution of the CP-conserving direct-photon emission process $K_L \to \pi^+\pi^-\gamma$ [14] from the inclusive measurement of $BR(K_L \to \pi^+\pi^-)$, we obtain $|\eta_\pm| = (2.219 \pm 0.013) \times 10^{-3}$. Finally, using the world average measurement of $\mathrm{Re}(\epsilon'/\epsilon) = (1.67 \pm 0.26) \times 10^{-3}$ and assuming $\arg \epsilon' = \arg \epsilon$, we obtain

$$|\epsilon| = (2.216 \pm 0.013) \times 10^{-3} \tag{8}$$

From Ref. 3 $|\epsilon| = (2.280 \pm 0.013) \times 10^{-3}$. A change on the central value of $\sim 3\%$ is observed.

Parameter	Value	Gaussian (σ)	Uniform (half-width)
λ	0.2258	0.0014	-
$\lvert V_{cb}\rvert$(incl.)	41.6×10^{-3}	0.7×10^{-3}	0.6×10^{-3}
$\hat{B}_K$	0.79	0.04	0.09
$\lvert\epsilon\rvert$	2.280×10^{-3}	0.013×10^{-3}	-
$\lvert\epsilon\rvert$ (KLOE)	2.216×10^{-3}	0.013×10^{-3}	-
f_K	0.159 GeV	fixed	
Δm_K	0.5301×10^{-2} ps^{-1}	fixed	
$\overline{m}_t$	165.0 GeV	3.9 GeV	-
$\overline{m}_c$	1.3 GeV	0.1 GeV	-
G_F	1.16639×10^{-5}GeV^{-2}	fixed	
m_W	80.425 GeV	fixed	
m_K^0	0.497648 GeV	fixed	

Table 3
Values of the quantities used to determine the constraint from the measurement of $|\epsilon|$ [18]. The Gaussian and the flat contributions to the uncertainty are given in the third and fourth columns respectively

The impact of this change on the determination of the unitarity triangle has been studied using:

$$|\epsilon| = C_\epsilon B_K A^2 \lambda^6 \bar{\eta} \left(-\eta_1 S_0(x_c)(1-\lambda^2) + \eta_3 S_0(x_c, x_t) + \eta_2 S_0(x_t) A^2 \lambda^4 (1-\bar{\rho}) \right) \quad (9)$$

where

$$C_\epsilon = \frac{G_F^2 f_K^2 m_K^0 m_W^2}{6\sqrt{2}\Delta m_K}$$

B_K is the so-called bag parameter which encodes the low energy QCD contribution to the $K^0 - \bar{K}^0$ mixing amplitude [15, 16], the quantities η_i are related to the short distance QCD corrections [15, 16], the S_0 are the so-called *Inami -Lim* functions [17] of $x_q = m_q^2/m_W^2$ (the ratio of the square mass of the quark q over the square mass of the W boson).

$|\epsilon|$ can be evaluated by using the experimental inputs reported in Ref. 18 as listed in Table 3 and the theoretical parameters η_i given in Ref. 16. For this purpose we use the computer program developed by the UTfit collaboration [18]. The regions allowed by the ϵ measurement in the plane (ρ, η) is shown in Fig. 14 at

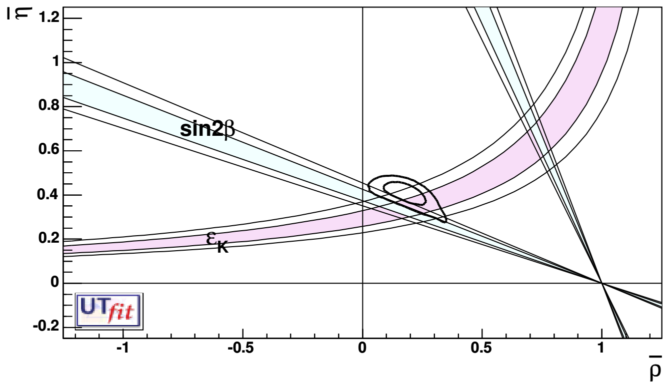

Fig. 14. Allowed regions for $(\bar{\rho}, \bar{\eta})$ (contours at 68% and 95%) as selected by the measurements of $|V_{ub}|/|V_{uc}|$, Δm_d and by the limit on Δm_s compared with the bands from the measurement of ϵ and $\sin 2\beta$ [18].

68% C.L. and the 95% C.L. The largest uncertainty is due in the computation of the parameter B_K. The constraints obtained from the measurement of sin2β and that obtained by combining the information from the CP conserving observables: $\Delta \mathrm{m_d}$, $\Delta \mathrm{m_s}$, V_{ub}, and V_{cb} are also shown in Fig. 14.
Alternatively the value of $|\epsilon|$ can be predicted. For this purpose we use the result reported in Ref. 18 where to test the mechanism of the CP violation in the Standard Model the value of $|\epsilon|$ has been computed from the measurement of the CP conserving observables: $\Delta \mathrm{m_d}$, $\Delta \mathrm{m_s}$, V_{ub}, and V_{cb}. The result of this study is shown in Fig. 15. No significant deviation from the standard Model prediction has been observed.

10 Conclusions

A new precise measurement of the $K_L \to \pi^+\pi^-$ branching ratio has been performed. The result:

$$(1.963 \pm \pm 0.012_{\mathrm{stat.}} \pm 0.017_{\mathrm{syst.}}) \times 10^{-3}$$

is in good agreement with the recent one obtained by KTeV [2], and in strong disagreement with that reported by the PDG, $(2.090 \pm 0.025) \times 10^{-3}$ [3]: A difference of 6% corresponding to $\sim$4 standard deviations is observed. The impact of this measurement on the dermination of the unitarity triangle apex has been studied and compared with determinations from measurements of other observables.

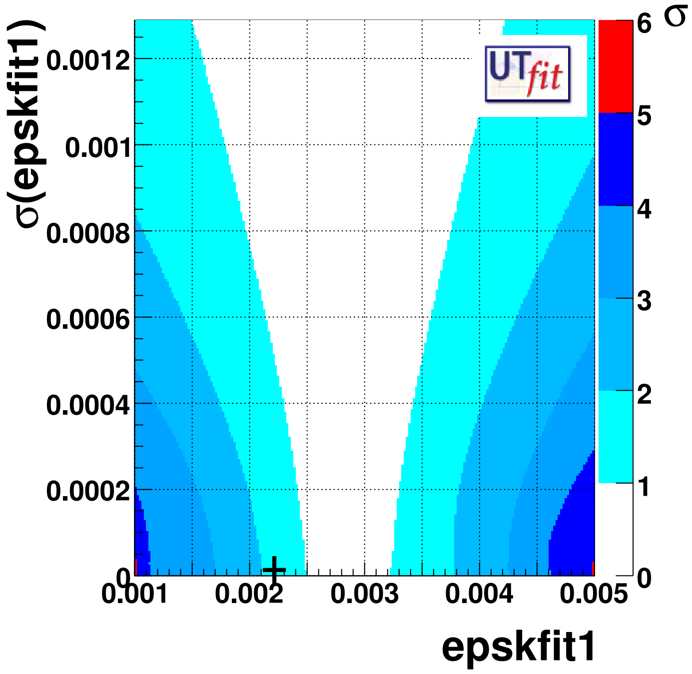

Fig. 15. $|\epsilon|$ constraints by the measurements of $|V_{ub}|/|V_{uc}|$, Δm_d and by the limit on Δm_son the $(\bar{\rho},\bar{\eta})$ from Ref. 18. compared with the value of $|\epsilon|$ from the measurements of $\mathrm{BR}(K_L\to\pi^+\pi^-)$.

A Evaluation of K_L BR's error matrix

Since we measure the ratio R=BR($K_L \to \pi^+\pi^-$)/BR($K_L \to \pi^\pm\mu^\mp\nu$) and the four dominant K_L absolute branching ratios, $BRa|_{\tau=51.54\ ns}$ with error matrix δBRa_{ij} , and we wish to transform to branching ratio measurements BR with the constraint $\sum BR = 1$ and lifetime τ:

$$\begin{aligned}
BR_i &= \tfrac{BRa_i}{\sum_i BRa_i}; \\
BR_5 &= BR(K_L \to \pi^+\pi^-) = R\ BR(K_L \to \pi^\pm\mu^\mp\nu) = R\ BR_2; \\
\tau &= 51.54 - \tfrac{\sum_i BRa_i - 1}{0.0128}
\end{aligned}$$

The transformation matrix is:

$$T = \begin{pmatrix}
\frac{dB_1}{dBa_1} & \frac{dB_2}{dBa_1} & \frac{dB_3}{dBa_1} & \frac{dB_4}{dBa_1} & \frac{dB_5}{dBa_1} & \frac{d\tau}{dBa_1} \\
\frac{dB_1}{dBa_2} & \frac{dB_2}{dBa_2} & \frac{dB_3}{dBa_2} & \frac{dB_4}{dBa_2} & \frac{dB_5}{dBa_2} & \frac{d\tau}{dBa_2} \\
\frac{dB_1}{dBa_3} & \frac{dB_2}{dBa_3} & \frac{dB_3}{dBa_3} & \frac{dB_4}{dBa_3} & \frac{dB_5}{dBa_3} & \frac{d\tau}{dBa_3} \\
\frac{dB_1}{dBa_4} & \frac{dB_2}{dBa_4} & \frac{dB_3}{dBa_4} & \frac{dB_4}{dBa_4} & \frac{dB_5}{dBa_4} & \frac{d\tau}{dBa_4} \\
\frac{dB_1}{dR} & \frac{dB_2}{dR} & \frac{dB_3}{dR} & \frac{dB_4}{dR} & \frac{dB_5}{dR} & \frac{d\tau}{dR}
\end{pmatrix}$$

The error matrix δB for the new set of measurements is derived from:

$$\delta B = T^T \delta Ba T$$

Using the values of BRa and δBRa_{ij} given in Ref. 12 and in section 7 we obtain:

$$\begin{pmatrix}
K_L \to \pi^\pm e^\mp\nu & K_L \to \pi^\pm\mu^\mp\nu & K_L \to \pi^+\pi^-\pi^0 & K_L \to \pi^0\pi^0\pi^0 & K_L \to \pi^+\pi^- & \tau_{K_L}(\text{ns}) \\
2.39\times10^{-6} & -0.57\times10^{-6} & -0.12\times10^{-6} & -1.71\times10^{-6} & -4.14\times10^{-9} & 1.36\times10^{-4} \\
 & 2.17\times10^{-6} & -0.35\times10^{-6} & -1.26\times10^{-6} & 1.59\times10^{-8} & 1.17\times10^{-4} \\
 & & 1.39\times10^{-6} & -0.91\times10^{-6} & -2.07\times10^{-9} & -1.64\times10^{-4} \\
 & & & 3.88\times10^{-6} & -1.02\times10^{-8} & -1.49\times10^{-4} \\
 & & & & 4.52\times10^{-10} & 8.57\times10^{-7} \\
 & & & & & 1.27\times10^{-1}
\end{pmatrix}$$

References

[1] J. H. Christenson, J. W. Cronin, V. L. Fitch, R. Turlay, Phys. Rev. Lett. 13 (1964) 138.

[2] KTeV Collaboration, T. Alexopolous, et al., Phys. Rev. D 70 (2004) 092006.

[3] Particle Data Group, K. Hagiwara, et al., Phys. Rev. D 66 (2002) 010001.

[4] N. Cabibbo, Phys. Rev. Lett. 10 (1963) 531.

[5] M. Kobayashi, T. Maskawa, Prog. Theor. Phys. 49 (1973) 652.

[6] KLOE Collaboration, F. Ambrosino, et al., Phys. Lett. B 632 (2006) 43.

[7] KLOE Collaboration, F. Ambrosino, et al., Phys. Lett. B 626 (2005) 15.

[8] M. Adinolfi, et al., The tracking detector of the KLOE experiment, Nucl. Instrum. Meth. A 488 (2002) 51.

[9] M. Adinolfi, et al., The KLOE electromagnetic calorimeter, Nucl. Instrum. Meth. A 482 (2002) 364.

[10] M. Adinolfi, et al., The trigger system of the KLOE experiment, Nucl. Instrum. Meth. A 492 (2002) 134.

[11] C. Gatti, Monte Carlo simulation for radiative kaon decays, hep-ph/0507280, accepted by Eur. Phys. J. C, and references therein .

[12] M. Antonelli, P. Beltrame, M. Dreucci, M. Moulson, M. Paultan, A. Sibidanov, Measurements of the Absolute Branching Ratios for Dominant K_L Decays, the K_L Lifetime, and V_{us} with the Kloe Detector, KLOE Note 204 (2005).
URL http://www.lnf.infn.it/kloe/pub/knote/kn204.ps.gz

[13] M. Palutan, T. Spadaro, C. Gatti, Precise measurement of $\Gamma(K_S \to \pi^+\pi^-)/\Gamma(K_S \to \pi^0\pi^0)$ with the KLOE detector at DAFNE, hep-ex/0601025 (2006)

[14] E. Ramberg, et al., Phys. Rev. Lett. 70 (1993) 2525.

[15] A. J. Buras, Probing the Standard Model of particle interactions, Les Houches, arXiv:hep-ph/9806471 (2001)

[16] G. Buchalla, et al., Rev. Mod. Phys. 68 (1996) 1225.

[17] T. Inami and C. S. Lim, Prog. Theor. Phys. **65**, 297 and 1772 (1981)

[18] M. Bona, et al., JHEP 07 (2005) 028.